# A framework for processing wave buoy measurements in the presence of current

# A framework for processing wave buoy measurements in the presence of current

A.C. Pillai[a,*], T. Davey[b], S. Draycott[c,*]

[a]*Renewable Energy Group, College of Engineering, Mathematics and Physical Sciences, University of Exeter, Penryn Campus, Penryn TR10 9FE, UK*

[b]*School of Engineering, FloWave Ocean Energy Research Facility, Institute for Energy Systems, The University of Edinburgh, Edinburgh EH9 3BF, UK*

[c]*Department of Mechanical, Aerospace and Civil Engineering, University of Manchester, Manchester M60 1QD, UK*

## Abstract

Waves and currents interact, with the resulting combination largely determining the loading on offshore structures and devices. Despite this, currents are often ignored and wave buoy data is processed without consideration of the current or the wave-current interaction. This data is subsequently used in design, yet sea state power, steepness, and directionality may have significant errors. Here we present a novel framework for the processing of wave buoy data to account for the effect of a current. We use a mesh adaptive direct search (MADS) algorithm to solve for the current and current-modified wave parameters simultaneously. Through 125 simulated directional wave-current sea states, we demonstrate the performance of the method under a wide range of conditions; including bimodal sea states with non-colinear current. Current speed and direction are estimated accurately for all cases (mean RMSE of $0.1179\,\mathrm{m\,s^{-1}}$ and 0.0091 rad respectively) which enables sea state steepness and power to be estimated within ±3%. Ignoring this current of $\pm 2\,\mathrm{m\,s^{-1}}$ when deriving these wave parameters results in errors up to 30%. This work demonstrates that it is possible to correctly process wave buoy measurement data to account for, and quantify, a current thus significantly reducing the uncertainty of the ocean conditions. After further validation work, the framework can be widely applied to historic datasets, correcting the wave data and providing an additional dataset of current velocities.

*Keywords:*
Wave-Current Interactions, Ocean Measurements, Mesh Adaptive Direct Search, Non-linear Programming, Wave Buoy Analysis, Directional spectra

## 1. Introduction

Both coastal and ocean environments experience waves and currents which have been shown to interact with one another to produce complex environmental conditions. These conditions must

*Corresponding author
*Email addresses:* a.pillai@exeter.ac.uk (A.C. Pillai), samuel.draycott@manchester.ac.uk (S. Draycott)

be considered when modelling and designing offshore structures, vessels, or devices as the loading and responses of these systems are governed by the environmental conditions. Wave kinematics have been shown to be altered by the presence of current [1, 2] and currents are affected by the presence of wave-induced velocities. Therefore, it is paramount that for accurate consideration of the environment in which offshore structures, vessels, or devices must operate in, that the combined behaviour and mechanisms for interactions are well understood and accurately characterized.

Wave buoys, traditionally deployed for marine weather forecasting, are the most widely used system for the measurement of ocean waves [3]. Large national wave buoy datasets are extensive, e.g. the National Buoy Data Centre [4] in the US have as of June 2020 archived 56,046 buoy months [5], and the Cefas WaveNet network of wave buoys in the UK has been operational since 2002 [6]. These datasets, along with targeted deployments, are commonly used to characterize the wave environment at sites of interest, including offshore renewable energy deployments, and to validate (and calibrate) numerical models which aim to cover wider areas and/or longer time frames. The resulting assessment of the wave climate; including wave heights, steepnesses, directions, and associated estimated extreme values are used as inputs for engineering design.

It has been frequently observed that wave buoy measurements are affected by currents [7–10]. Recognising this issue, buoys have recently been developed to capture both waves and currents; including the TRIAXYS with Currents Buoy [11], and surface kinematics buoys [12]. However, historical datasets do not contain this information and the vast majority of installed wave buoys do not have the capability to measure, and account for, the presence of a current. The presence of an unknown current introduces a number of errors, of different categories, in the wave buoy measurement-analysis approach:

**Category 1:** *Wave climate misrepresentation*: Currents affect the wave heights, lengths, and velocities [13]. The modified wave heights are captured by the buoy without the corresponding changes to wavelength and velocities, and hence the inferred power and steepness of the sea states are incorrect

**Category 2:** *Errors in direction*: The standard approaches for estimating wave directions and directional spreading from wave buoys do not work in the presence of a current (can be inferred from [14, 15]) as wavenumbers are now unknown and a function of the direction relative to the current field. Standard approaches will misrepresent the directional spreading and mean directions of the sea states.

**Category 3:** *Alteration to buoy dynamics*: The current provides a mean force on the buoy and increases the tension in the mooring line. This in turn, alters the dynamics (and appropriate response functions) of the buoy and its ability to surface track, likely underestimating the sea surface elevation.

In addition to errors in the estimation of wave properties, a current also applies a mean force on any offshore system, and hence is a parameter of significant importance for engineering design which requires quantification.

This paper addresses Category 1 and 2 errors above by developing an improved buoy analysis approaches to estimate, and account for, the presence of a current. This is a problem which has not

been addressed to date to the knowledge of the authors. The published work assessing the effect of current on wave buoy measurement errors does so by neglecting the wave-current interaction entirely; finding that there are still errors introduced by the presence of current in estimates of both mean wave direction and spectral form [16].

The present work develops a framework for processing wave buoy measurements in the presence of current, thus enabling the isolation of the wave directional spectra and the underlying current field. To achieve this, the measured cross-spectra between the wave buoy measurement signals are combined with a theoretical formulation of how an arbitrary current velocity impacts these cross-spectra based on linear wave-current interaction theory in the presence of a steady and uniform current.

To isolate this impact of the current, the framework approaches this as a *parameter estimation* optimization problem. Optimization algorithms in general seek the best possible combination of variable values amongst all those available. All optimization algorithms require the problem to be represented using an evaluation function which judges the relative quality of the proposed solutions with a search algorithm then being deployed to minimize or maximize this function [17]. Parameter estimation problems are the class of optimization problems in which an optimization algorithm is deployed to fit parameters to data, in this case the problem seeks the parameters that most accurately reconstruct the wave and current regime by minimizing the error between the estimated (i.e. reconstructed) cross-spectra and those measured. Parameter estimation problems have been well studied for a wide range of engineering applications [18–20] including applications specific to offshore renewable energy [21].

The presented framework, and its application to simulated datasets, demonstrates the framework's potential to both reprocess existing wave buoy datasets and to be integrated into wave buoy processing methods. This will subsequently account for any potential currents and their impact on the characterisation of the underlying wave systems.

The article is laid out as follows: Section 2 presents the underlying wave-current interaction theory, simulation methods, and mesh adaptive direct search (MADS) optimization algorithm which is used to resolve the wave and current systems. Section 3 presents the numerical simulations used to test and demonstrate the framework's capabilities followed by further discussion in Section 4. Concluding remarks are offered in Section 5.

## 2. Theory and Methodologies

This section briefly describes the fundamental theory underpinning the problem at hand, the methodology deployed to resolve it, and the approach used to test the performance. The modification of wavenumber by current and hence the misrepresentation of power and steepness is presented in Section 2.1. The relationship between cross-spectra and directional spectra is detailed in Section 2.2, along with how standard processes to infer the directional spectra introduce errors if currents are present. In order to test the newly developed framework for resolving these errors, a simplified method for simulating the motions of a perfect surface tracking wave buoy in current is presented in Section 2.3. Finally, the optimization framework used to account for the current in the analysis procedure is presented in Section 2.4.

### 2.1. Wave Climate Misrepresentation: Modification of Waves by Current

As mentioned in Section 1, the presence of a current modifies the wavenumbers (wave lengths), wave heights and associated velocities. Assuming that wave buoys measure the surface elevation accurately, and hence wave heights, incorrect assumptions about the wavenumber, by ignoring the presence of current, introduce errors in the calculated wave climate (Category 1 errors).

In the presence of a steady and uniform current the wavenumber is a function of frequency, depth, current speed, and angle relative to the current field. The dispersion relation can be written as [22]:

$$\omega - kU\cos\zeta = \omega_r = \sqrt{gk\tanh kh} \tag{1}$$

where $U$ is the current speed, $\omega$ is the angular frequency in the fixed reference frame and $\omega_r$ is the angular frequency observed in a reference frame moving with the mean current. $k$ is the wavenumber, $h$ is the water depth, and $g$ is the acceleration due to gravity. $\zeta$ is the relative angle between the wave and current fields, where $\zeta = 0$ for waves travelling on a following current.

The group velocity, $C_g$, is given by:

$$C_g = \frac{C}{2}\left(1 + \frac{2kh}{\sinh(2kh)}\right) \tag{2}$$

where $C = \omega/k$ is the phase speed in the fixed reference frame.

If $U$ is assumed to be zero then there will be errors in $k$ and $C_g$ which consequently introduce errors in the assumed sea state steepness and power respectively. These are critical parameters for understanding the hydrodynamic response of offshore systems; and in the case of wave power the energy yield and system performance.

Figure 1 demonstrates the relative errors in steepness and power for a range of wave frequencies and relative current velocities for $h = 25\,\mathrm{m}$. It can be observed that at relative velocities of $\pm 2\,\mathrm{m\,s^{-1}}$, the steepness and power can be misrepresented by greater than $\pm 40\%$.

### 2.2. Errors in Direction: Calculating Directional Spectra from Cross-Spectra

Cross-spectra between measured signals obtained from wave buoys are used in combination with a directional spectrum reconstruction method to estimate the directional spreading function, for each frequency component (e.g. [14]). The cross-spectra – along with the directional Fourier coefficients often provided from buoy measurements – are influenced by the current modification to the wavenumber (Eq. (1)), yet this is ignored in standard wave buoy processing methodologies (Category 2 errors). Specifically, the wavenumber is assumed to be independent of angle and to follow the standard dispersion relation, which is no longer the case in the presence of current.

The directional spectrum, $E(f,\theta)$, can be expressed as:

$$E(f,\theta) = S(f)D(f,\theta) \tag{3}$$

where $D(f,\theta)$ is the directional spreading function (DSF) and $S(f)$ is the frequency spectrum.

The cross-spectra, $G_{m,n}$ of signals $m$ and $n$ are related to the directional spectrum $E(f,\theta)$ by [23, 24]:

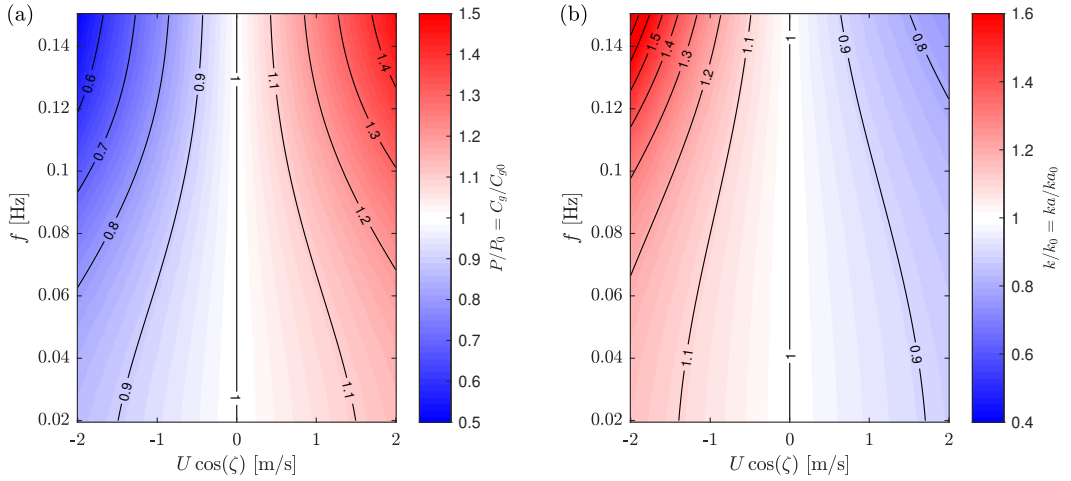


**Figure 1:** Relative errors in (a) sea state power and group velocity, and (b) sea state steepness and wavenumber, if current is ignored (subscript 0) for a range of frequency and relative current velocities. Water depth, $h$, set to 25 m.

$$G_{m,n}(f) = \int_0^{2\pi} H_m(f,\theta) H_n^*(f,\theta) e^{-i\vec{k}(\vec{x_n}-\vec{x_m})} E(f,\theta) d\theta \tag{4}$$

Where $H_m$ and $H_n$ are the transfer functions relating signals $m$ and $n$ respectively to the equivalent surface elevation (assuming linear wave theory).

This can be re-written in terms of the frequency spectrum, $S(f)$, and the directional spreading function, $D(f,\theta)$, based on the relationship in Eq. (3):

$$G_{m,n}(f) = S(f) \int_0^{2\pi} H_m(f,\theta) H_n^*(f,\theta) e^{-i\vec{k}(\vec{x_n}-\vec{x_m})} D(f,\theta) d\theta \tag{5}$$

For co-located signals, such as those measured by wave buoys, this can be reduced to:

$$G_{m,n}(f) = S(f) \int_0^{2\pi} H_m(f,\theta) H_n^*(f,\theta) D(f,\theta) d\theta \tag{6}$$

For a heave-surge-sway buoy, as simulated in Section 2.3, $m$ is in the range 1 to 3 representing heave ($z$), surge ($x$), and sway ($y$) respectively. If current is incorporated properly as a function of angle, the corresponding transfer functions are:

$$H_1 = 1 \tag{7}$$

$$H_2 = i \frac{\cos\theta}{\tanh k(f,\theta) d} \tag{8}$$

$$H_3 = i \frac{\sin\theta}{\tanh k(f,\theta) d} \tag{9}$$

where $k$ is a function of the angle (current velocity) and calculated through Eq. (1). Hence, the formulation of the cross-spectra includes the current-modified wavenumbers and the directional spectrum; the parameters required to infer all wave and current information. This is the formulation used in Section 2.4 to obtain the correct values for $k$, $U$ and $D(f,\theta)$ from measured cross-spectra.

### 2.2.1. Errors in standard processing methodologies

As detailed in Benoit et al. [14], standard processing techniques assume that $k$ is not a function of angle, and hence when solving for $D(f, \theta)$ it is assumed that $k$ can be brought outside of the integral over direction in Eq. (6). $k$ is then also calculated using the standard dispersion relation (Eq. (1) with $U$ set to 0). In the presence of current, these assumptions cause errors in the calculated directional spectrum, regardless of the method choice.

Some directional spectrum reconstruction methods use directional Fourier coefficients rather than the cross-spectra. As such, these are often provided from buoy measurements. These are related to $D(f, \theta)$ by:

$$D(f, \theta) = \frac{a_0}{2\pi} + \frac{1}{\pi} \sum_{n=1}^{\infty} a_n \cos(n\theta) + b_n \sin(n\theta) \tag{10}$$

The Fourier coefficients are typically obtained through combinations of cross-spectra by relating Eq. (6) to Eq. (10). The (incorrect) assumption that $k$ can be brought outside of the integral makes this straightforward, noting that the transfer functions also contain $\cos\theta$ and $\sin\theta$ terms.

To obtain representative estimates of the likely errors in mean direction and spreading resulting from the assumption that there is no current, theoretical cross-spectra have been generated for a heave-surge-sway buoy for uni-model sea states, including various current velocities and relative angles. A widely used $D(f, \theta)$ formulation is presented later in Section 2.3.1, and Eq. (13) is used to generate the directional spectrum, with Eqs. (6) to (9) used to subsequently calculate the theoretical cross-spectra. For convenience, when estimating these likely errors, rather than reconstructing the full directional spectra from the generated cross-spectra, rank 1 estimates of the mean direction, $\theta_0$, and the directional spread, $s$, from the standard Mitsuyasu model [25] are obtained using:

$$s = \frac{r_1}{1 - r_1} \tag{11}$$

$$\theta_0 = \arg(a_1 + ib_1) \tag{12}$$

where $r_n = \sqrt{a_n^2 + b_b^2}$, $a_n$ and $b_n$ are defined in Eq. (10) and are calculated from the cross-spectra making the normal assumption that $k$ is independent of angle (see e.g. [14, 26]). The calculated values of $s$ and $\theta_0$ can be compared the the input to Eq. (13) in order to assess the error.

Figure 2 shows the expected errors $s$ and $\theta_0$ for a range of relative current velocities, frequencies, and angles between the mean wave direction and the current. When waves follow or oppose the current direction ($\theta_0 = 0, \pm\pi$) it is evident that there are no errors in the estimate of the mean direction, yet the errors are largest for the spread. Very low errors are expected in the spread when the mean wave direction is perpendicular to the current, yet this represents the angle where the errors in mean direction are largest. Nevertheless, it is apparent that the errors in both of these parameters are very small regardless of the current or relative angle. This is of key importance to the problem as these are essentially just a function of the cross-spectra between the signals, and it is these cross-spectra that are used here to resolve the directional wave field. Hence, only small differences in the cross-spectra are relied upon to infer the current.

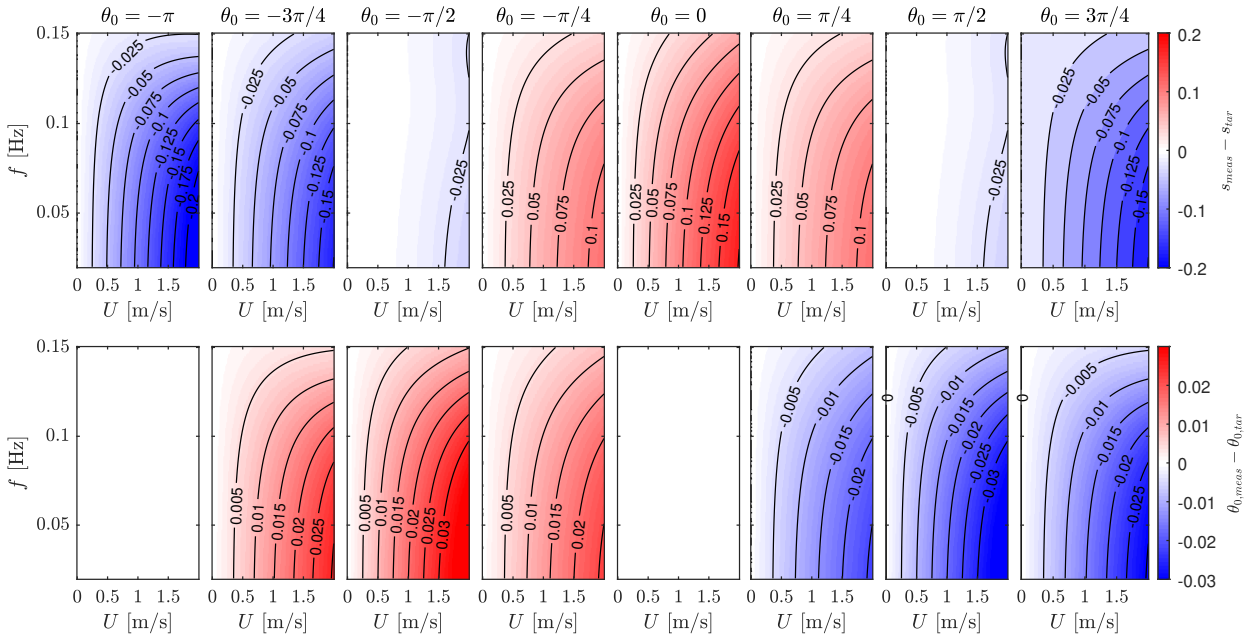


**Figure 2:** Errors in (top row) directional spreading, and (bottom row) mean direction, if current is disregarded for a range of frequency, current velocity and relative angles. Current direction, $\beta$, is set to 0 rad, $h = 25$ m, and $s = 5$.

### *2.3. Simulation of A Perfect Surface Tracking Buoy*

This section describes a simplified method of simulating the buoy motions in directional wave fields in the presence of current. The specification of conditions is detailed in Section 2.3.1, including the directional spreading function used. Section 2.3.2 describes how buoy motions are simulated to represent those experienced in the current-modified directional wave conditions, and briefly outlines the method of calculating the cross-spectra from the simulated time-series.

#### *2.3.1. Condition Specification*

To test the optimization approach for solving directional wave current fields (Section 2.4) sea states need to be simulated. Throughout this work we use the JONSWAP formulation for the energy distribution across frequency, $S(f)$, with a peak enhancement factor, $\gamma$ of 3.3 [27].

To enable generation and assessment of complex directional combined wave-current fields a Bimodal Mitsuyasu Model formulation is used for the directional spreading. The Mitsuyasu Model [25] is commonly used in the description of real seas, and the use of the bimodal variation adds flexibility allowing it to be more widely applied. Here, $D(f,\theta)$ is approximated using a bimodal cosine-2s, commonly referred to as cos-2s, formulation. Compared to the original cos-2s formulation the present formulation introduces three additional parameters ($\lambda$, $s_2$, and $\phi_0(f)$) in order to allow greater flexibility and allow the formulation to represent a wider set of directional spreading functions.

The extension to a bimodal formulation approximates the directional spreading function as a superposition of two cos-2s functions with an additional weighting parameter, $\lambda$ [28]. The bimodal formulation is given in Eq. (13). Setting this weighting parameter to a value of 1 removes the influence of the second system ($s_2$ and $\phi_0(f)$) and reduces the expression to the traditional

Mitsuyasu Model. $\lambda$ values of 0 likewise remove the influence of the first system and also reduce the expression to unimodal.

$$D(f,\theta) = \lambda \cdot \left( R(f) \cos^{2s_1}\left[\frac{\theta - \theta_0(f)}{2}\right]\right) + (1-\lambda) \cdot \left( R(f) \cos^{2s_2}\left[\frac{\theta - \phi_0(f)}{2}\right]\right) \tag{13}$$

where the subscript 1 denotes the first constituent cos-2s system, and the subscript 2 denotes the second constituent system. Note that all parameters are frequency dependent, and hence the spreading function can vary greatly with frequency. This parameterization is used both to generate the wave fields, and later when fitting an estimated directional spectrum.

The term $R(f)$ is defined by:

$$R(f) = \frac{2^{2s(f)}\Gamma^2(s(f)+1)}{2\pi\Gamma(2s(f)+1)} \tag{14}$$

This bimodal formulation gives rise to a wide range of possible spreading functions as demonstrated in Fig. 3, and hence can be used to represent the majority of measured sea states effectively.

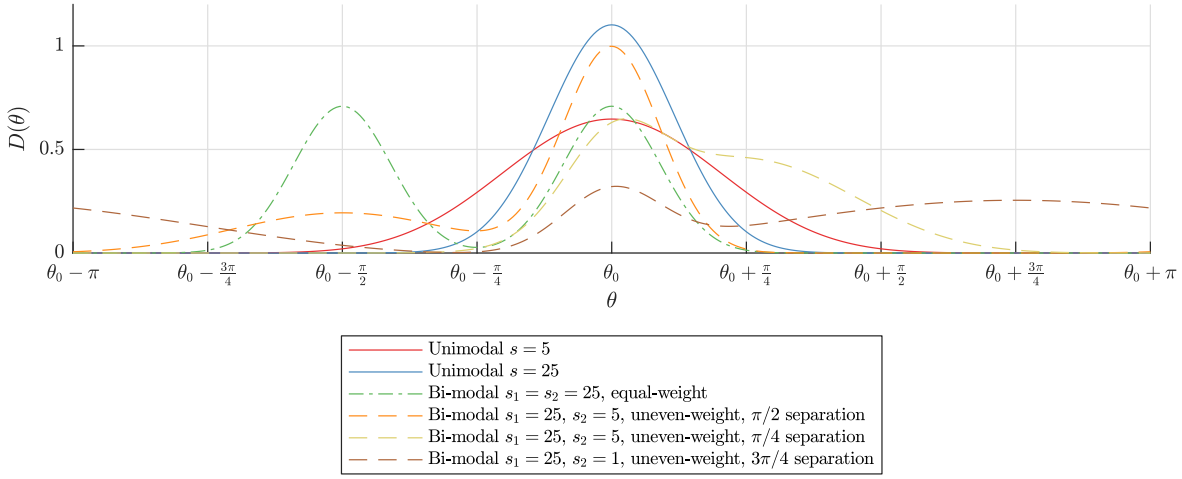


**Figure 3:** Cos-2s directional spreading functions using the Bimodal Mitsuyasu Model

JONSWAP frequency spectra, $S(f)$ along with the Mitsuyasu model for $D(f,\theta)$ have been chosen due to their frequent use in describing, modelling, and analysing sea states. JONSWAP spectra offer the ability to change the bandwidth, whilst the bimodal Mitsuyasu model used allows for the representation of complex directional distributions which other models cannot describe. This combination hence offers a wide range of possibilities for trialling the proposed methodology detailed in Section 2.4.

### *2.3.2. Buoy Motion Simulation*

A simplified approach is taken to simulating the buoy motion, assuming that it behaves as a perfect surface tracking buoy and hence follows the wave-induced particle trajectories, but not

that of the current. In addition to linear wave theory, this essentially assumes that radiation and diffraction effects are negligible, and that the mooring system station-keeps without providing a restoring force observed at the wave frequencies. The implications of this, and hence areas for further work, are discussed in Section 4.

Assuming linear wave theory, the surface elevation time-series at an $[x, y]$ location can be described as a double sum of sinusoidal wave components over frequency and direction:

$$\eta(x, y, t) = \sum_{j=0}^{N_f} \sum_{m=0}^{N_\theta} a_{j,m} \cos(k_{j,m}(x \cos\theta_{j,m} + y \sin\theta_{j,m}) - \omega_j t + \Phi_{j,m}) \tag{15}$$

where amplitudes are related to the directional spectrum via $a_{j,m} = \sqrt{2E_{j,m}\Delta f \Delta\theta}$. $E_{j,m}$ is the energy density for frequency component $j$ and directional component $m$, and similarly $k_{j,m}$ is the component wavenumber. $\Phi_{j,m}$ is a random phase which is uniformly distributed between 0 and $2\pi$. $\Delta f$ and $\Delta\theta$ are the frequency and directional spacings used. $N_f$ and $N_\theta$ are the number of frequency and direction components respectively.

However, to simulate sea states which are ergodic, avoiding phase locking, the single-summation method is used [29]. Here the wave components are re-mapped to ensure that each frequency is assigned only one direction, and the directional spread ensured over each $N_\theta$ frequencies. This method of simulating directional sea states is described in detail in Draycott et al. [30, 31]. The single-summation form of the surface elevations become:

$$\eta(x, y, t) = \sum_{j \in \mathbb{F}} a_j \cos(k_j(x \cos\theta_j + y \sin\theta_j) - \omega_j t + \Phi_j) \tag{16}$$

where $j \in \mathbb{F}$ and $\mathbb{F}$ is the set of frequency components. The horizontal particle displacements, at the surface, can be expressed as:

$$\Delta x(x, y, t) = \sum_{j \in \mathbb{F}} \frac{a_j \cos(\theta_j)}{\tanh(k_j d)} \sin(k_j(x \cos\theta_j + y \sin\theta_j) - \omega_j t + \Phi_j) \tag{17}$$

$$\Delta y(x, y, t) = \sum_{j \in \mathbb{F}} \frac{a_j \sin(\theta_j)}{\tanh(k_j d)} \sin(k_j(x \cos\theta_j + y \sin\theta_j) - \omega_j t + \Phi_j) \tag{18}$$

In Fourier space the following can be defined (for ease, setting $x = y = z = 0$):

$$A_{\eta_j} = a_j e^{i\Phi_j} = c_j \qquad \forall j \in \mathbb{F} \tag{19}$$

$$A_{\Delta x_j} = i\frac{c_j \cos(\theta)}{\tanh(k_j d)} \qquad \forall j \in \mathbb{F} \tag{20}$$

$$A_{\Delta y_j} = i\frac{c_j \sin(\theta_j)}{\tanh(k_j d)} \qquad \forall j \in \mathbb{F} \tag{21}$$

where $c_j$ is the complex Fourier coefficient, incorporating phase $\Phi_j$ for frequency component $j$.

To rapidly simulate time-series of $x$, $y$ and $z$ displacements for a given directional sea state an Inverse Fast Fourier Transform (IFFT) can be applied to Eqs. (19) to (21).

As will become apparent in Section 2.4, the cross-spectra, i.e. the cross-covariance spectral densities between each measurement couple [26], are calculated from the simulated buoy motions and used in combination with the theoretical formulation presented in Section 2.2 (Eq. (6)), to calculate the directional spectrum and current velocity. Cross-spectra are calculated using MATLAB, with $N_\theta$ windows to ensure the cross-spectral densities in each frequency bin are representative of the directional spread. To estimate sea state parameters, the error between these calculated cross-spectra, and those from a theoretical formulation are minimized.

### *2.4. Optimization Framework*

#### *2.4.1. Optimization by Pattern Search*

Equations (6) to (9) describe the impact that currents have on a theoretical wave buoy with a station-keeping mooring. Using this formulation, it is possible to restructure the governing equations to relate the cross-spectra of the measured signals to the incident wave field and the incident current; thereby allowing a decomposition of the measurements to components defining the wave field and components defining the current. This decomposition process is achieved by restructuring the problem as a *parameter estimation problem* in which an optimizer selects parameters defining the wave and current regime, searching for the parameter combination which minimizes the error between the parameterized, estimated cross-spectra and the measured cross-spectra.

Parameter estimation, those optimization problems which seek to fit a model to measurements, for a system involving many variables which may have complex relationships to one another, can be addressed using an optimization approach in which the objective function represents an error function between the model and the measurements. For such approaches, many optimization algorithms may be relevant. For problems with complex relationships between the parameters being estimated, in this case the parameters describing the wave field and current velocity, with functions which cannot be easily differentiated, heuristic algorithms such as the genetic algorithm or particle swarm would be appropriate. These algorithms, however, suffer in scenarios with complex constraints as the constraints must either be incorporated into the objective function as a penalty function, or a post-processing "repair" function is necessary to correct solutions to ensure that all constraints are satisfied [32–34]. Direct search algorithms on the other hand, are capable of handling complex objective functions that are not differentiable and simultaneously deal with generalized non-linear constraints [35, 36].

In previous work, interior-point optimization methods such as IPOPT [37–39] have been deployed for parameter estimation of current-affected wavenumbers, as this can be formulated as a convex non-linear programming function with differentiable objectives and constraints [2]. Gradient methods, a broad family of optimization algorithms including interior-point methods and IPOPT, while computationally efficient, do suffer from convergence to local solutions rather than

global solutions. Therefore these methods can struggle given especially complex objective spaces where direct search algorithms such as mesh adaptive direct search (MADS) [40] could be more successful. The present work, therefore adopts the non-linear implementation of MADS distributed as the *Non-linear Optimization by Mesh Adaptive Direct Search (NOMAD)* software package [41].

Strictly speaking, the MADS algorithm can be classed as a pattern search algorithm, a family of algorithms which use a pattern to determine trial points. All pattern search algorithms are characterized by not being gradient based, and therefore do not require any information about the gradient of the objective function or constraint functions, and they do not attempt to develop an approximate of these gradients. Compared to the generalized pattern search (GPS), the MADS algorithm is characterized by a sophisticated method of generating the mesh (i.e. trial points) around the current point to test [40, 42, 43]. The NOMAD implementation of MADS and MADS in general are well suited to problems of few variables, but with expensive evaluation functions [41].

MADS is a black box optimization solver which can solve optimization problems of any form including non-linear optimization problems in the general form:

$$\begin{aligned} \min \quad & f(x) \\ \text{s.t.} \quad & g^L \leq g(x) \leq g^U \\ & x^L \leq x \leq x^U \end{aligned}$$

where $x$ is the vector of decision variables; $f(x)$ is the convex objective function to be minimized; $g^L$ and $g^U$ are respectively the lower and upper bounds on the constraint function $g(x)$; and $x^L$ and $x^U$ are respectively the lower and upper bounds on the decision variables.

### *2.4.2. Optimization Problem Formulation*

In the present problem, for each frequency and pair of degrees of freedom, there exists one cross-spectral value denoted by $G_{m,n}(f)$ where $f$ is a frequency component belonging to the set of frequencies $\mathbb{F}$, and $m$ and $n$ are two degrees of freedom. In the present case $m$ and $n$ are in the range $1-3$ representing heave, surge, and sway respectively. In the optimization problem, the subscripts $o$ and $e$ denote *observed* and *estimated* respectively. The observed values refer to those from the buoy while the estimated spectra are those defined by fitting parameters using Eq. (27). The objective function which the optimizer seeks to minimize is therefore the sum of differences between the observed and estimated cross-spectral values. As the cross-spectra are complex, this complex error is multiplied by the conjugate ($^*$) to regularize this error term.

Each frequency of the spectra are considered independently and solved as a separate optimization problem. Solving frequency by frequency allows the optimization problem to be reduced to a series of smaller problems with lower computational complexity involving smaller search spaces. Assuming linear wave theory, there are no interaction effects between the different frequencies, and therefore this reduction of the larger problem into a series of optimization problems does not impact the optimal solutions. Given the MADS algorithm's sensitivity to the size of the problem, reducing the problem in this way also enables the MADS algorithm to be deployed.

Figure 4 shows the overarching approach of the proposed framework for processing wave buoy measurements. The optimization problem is highlighted in a yellow box, is solved for each frequency component of the frequency spectrum, and is formulated using Eqs. (22) to (27).

$$\min \quad ln\left(\sum_{m=1}^{3}\sum_{n=m}^{3}\left(\left[\left(G_{m,n}(f)\right)_o - \left(G_{m,n}(f)\right)_e\right]\cdot\left[\left(G_{m,n}(f)\right)_o - \left(G_{m,n}(f)\right)_e\right]^*\right)\right) \tag{22}$$

$$\text{s.t.} \quad D(f,\theta) = \lambda(f)\cdot\left(R(f)\cos^{2s_1(f)}\left[\frac{\theta-\theta_0(f)}{2}\right]\right) + (1-\lambda(f))\cdot\left(R(f)\cos^{2s_2(f)}\left[\frac{\theta-\phi_0(f)}{2}\right]\right) \tag{23}$$

$$C_0(f) - U(f)\cdot\cos(\theta-\beta(f)) > 0 \tag{24}$$

$$2\pi f - k(f,\theta)\cdot U(f)\cos\left(\theta-\beta(f)\right) = \sqrt{gk(f,\theta)\tanh(k(f,\theta)h)} \tag{25}$$

$$H(f,\theta) = \left[1, i\frac{\cos\theta}{\tanh k(f,\theta)d}, i\frac{\sin\theta}{\tanh k(f,\theta)d}\right] \tag{26}$$

$$\left(G_{m,n}(f)\right)_e = S(f)\int_0^{2\pi} H_m(f,\theta)H_n^*(f,\theta)D(f,\theta)d\theta \qquad \forall\{m,n\}\in\{1,2,3\} \tag{27}$$

In the above formulation, Eq. (22) gives the objective function which is to be minimized by the optimizer. This function defines the error between the observed cross-spectra and those defined by the fit parameters. In an effort to avoid especially small objective values which can cause numerical instabilities for the optimizer, a log-transformation is applied to the error values. This transformation shifts the objective function such that rather than a target value of 0, the optimizer is now attempting to achieve $-\infty$. Equation (23) constrains the form of the directional spreading function (DSF) to be of a bimodal cos-2s form defined as defined in Eq. (13). For each frequency, this is therefore defined by 5 parameters (2 spreads, 2 mean directions, and a relative weight). Equation (24) constrains the current velocity at a given direction to not exceed the phase velocity to ensure that the waves are not blocked. Equation (25) defines the relationship between the current-altered wavenumbers ($k(f,\theta)$) and the current as given by linear wave theory (Eq. (1)). Equations (26) and (27) give the equations for the buoy transfer functions and the general expression for the estimated cross-spectra as defined in Eqs. (6) to (9) in Section 2.

As the problem is solved frequency by frequency, the optimizer therefore considers only seven continuous decision variables in each optimization problem to solve. These are defined in Table 1 along with the upper/lower bound constraints, and the initial guess provided to the optimizer for the first frequency component. As the search process is sensitive to the initial guess, an arbitrary guess of 1 or 0 was supplied to the optimizer for the first frequency component. For each subsequent optimization problem the initial guess was set to the optimal solution found for the previous frequency component.

## 3. Numerical Testing

### *3.1. Test Overview*

To test and explore the capabilities of the devised framework, a series of simulations were executed simulating the behaviour of a buoy, its measurements, and then using the framework as described in Section 2.4.2 to estimate the underlying wave parameters, current velocity, and therefore the current-affected wavenumbers ($k$) based on the synthetic buoy measurements. A total of 125 simulations both with and without current were executed. Initially, the framework

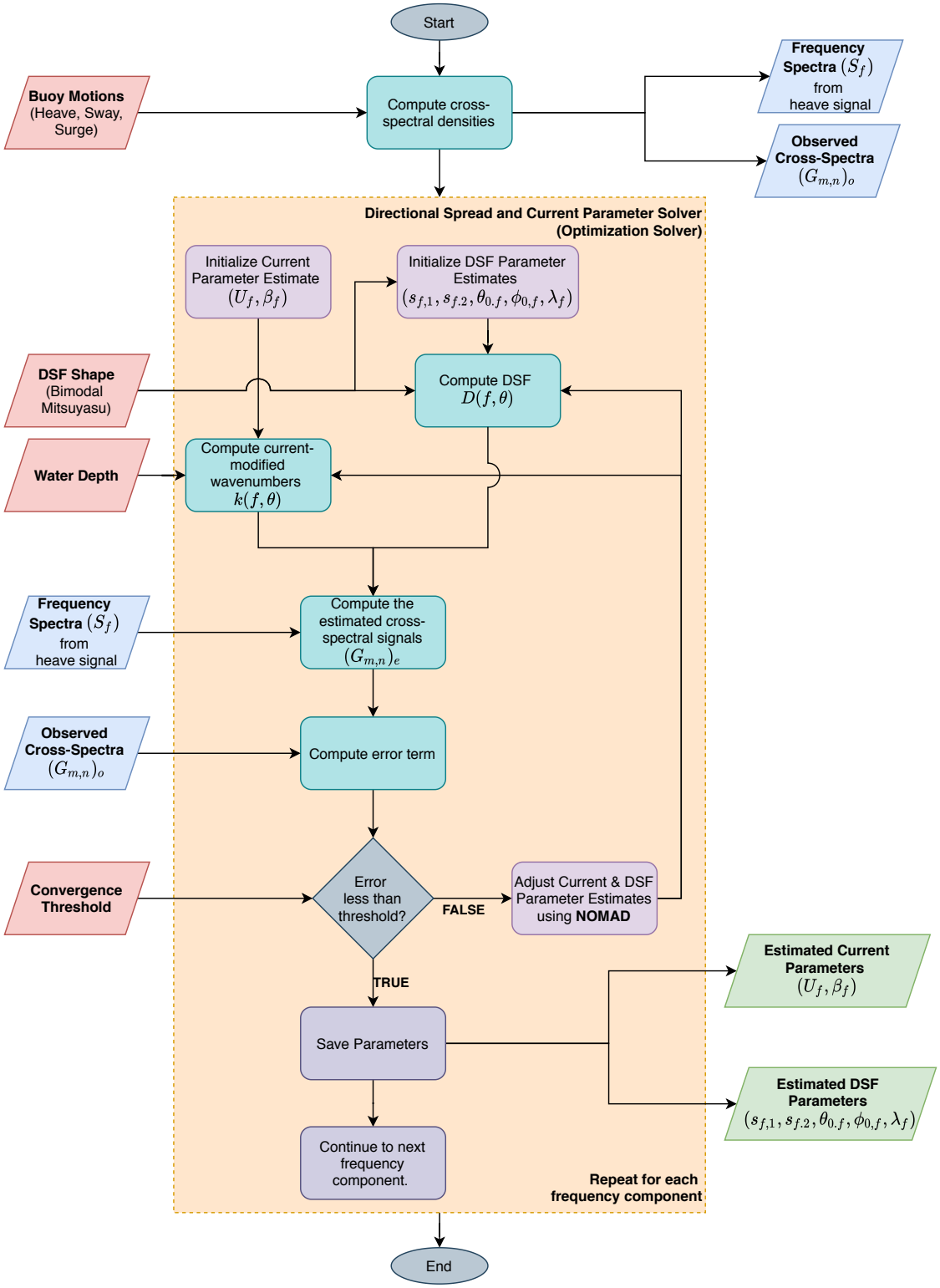


**Figure 4:** Generalised methodology of the framework. In this diagram, the core inputs including the buoy measurements, the water depth, a DSF parameterization/shape, and a convergence threshold are shown in red. The main optimization loop solved for each frequency component is shown in the yellow box. The output parameters describing the wave spreading and underlying current are shown in green.

**Table 1:** Definition of the decision variables of the optimization problem

| Parameter | Description | Type | Bounds | Optimizer Start |
|---|---|---|---|---|
| $s_{f,1}$ | Spread of first mode | Continuous | $0 \leq s_{f,1} \leq 50$ | 1 |
| $s_{f,2}$ | Spread of second mode | Continuous | $0 \leq s_{f,2} \leq 50$ | 1 |
| $\theta_{0,f}$ | Mean direction of first mode | Continuous | $0 \leq \theta_{0,f} \leq 2\pi$ | 1 |
| $\phi_{0,f}$ | Mean direction of second mode | Continuous | $0 \leq \phi_{0,f} \leq 2\pi$ | 1 |
| $\lambda_f$ | Relative weight of first mode | Continuous | $0 \leq \lambda_f \leq 1$ | 0 |
| $U_f$ | Current speed | Continuous | $U_f \geq 0$ | 0 |
| $\beta_f$ | Current direction | Continuous | $-\pi \leq \beta_f \leq \pi$ | 1 |

was benchmarked in no current to compare its performance in wave-only conditions against established methodologies. Similarly, the method's capabilities for multi-modal directionally spread seas was also verified prior to a detailed study in unimodal seas as outlined in Table 2. To reduce the number of cases considered, the current direction was fixed and only the wave direction was altered, however, importantly, the framework solves for both the wave and current directions.

**Table 2:** Parameters of Numerical Simulations

| Parameter | Symbol | Base Value | Sensitivity |
|---|---|---|---|
| Wave Height | $H_s$ | 4 m | - |
| Wave Period | $T_p$ | 9.5 s | 5 s to 20 s |
| Peak Enhancement Factor | $\gamma$ | 3.3 | - |
| Directional Spread | $s$ | 5 | 5 to 25 |
| Mean Wave Direction | $\theta_0$ | $\frac{\pi}{4}$ rad | 0 rad to $\pi$ rad |
| Current Speed | $U$ | 0 m s$^{-1}$ | 0 m s$^{-1}$ to 2 m s$^{-1}$ |
| Current Direction | $\beta$ | 0 rad | - |

Note that the value of $H_s$ is not varied as the wave-current interaction is modelled as linear and the choice of $H_s$ does not affect the ability to compute the directionality. Additionally, the frequency spectrum, and hence $H_s$, is readily computed directly from the heave measurements and as such the $H_s$ values modelled is inconsequential. Similarly, $\gamma$ is also not varied as the method has low sensitivity to spectral shape in its own right (effectively defining the component amplitudes at specific frequencies). It is, however, sensitive to the frequencies present, as the wave-current interaction effects result from their associated velocities relative to the current field. $T_p$ and $\theta_0$ are varied to capture this sensitivity, along with $U$. The current direction, $\beta$ is not varied as it is the relative angles between the wave and current fields which affect performance.

For each set of conditions "theoretical" cross-spectra were generated based on the relationship between the cross-spectra, the directional spreading function (DSF), the frequency spectra, and the transfer functions. This included consideration of how the presence of a current affected the wavenumbers ($k$) which are included in the transfer functions. A second set of cross-spectra were also generated by simulating a perfect surface tracking buoy, and using the displacements

to compute cross-spectra. This second-set are referred to as "time-series" as they are based on a time-series recreation of a sea surface elevation as described in Section 2.3.2.

Directional spectra outputs are compared to those obtained using the maximum entropy principle (MEP) using Newton's method of local linearization [44]. This approach effectively treats $D(f,\theta)$ as an unknown circular probability density function (PDF). The PDF is solved for using the principle of entropy, $En$:

$$En = -\int_0^{2\pi} D(f,\theta)\ln D(f,\theta)d\theta \tag{28}$$

The principle of maximum entropy states that the PDF which best represents the underlying distribution maximises Eq. (28). This is accomplished by solving for a series of unknown Lagrange multipliers, and can be further linearized using Newton's method of local linearization as detailed in [44]. This is the approach implemented in this work for comparison to the newly developed method.

### *3.2. Unimodal Directional Spreading with No Current*

The base case simulations described in Table 2 were used to simulate a perfect surface tracking buoy as described in Section 2. In total 19 cases were run without current varying the spread of the directional spectrum and the peak period of the frequency spectrum ($T_p$). Figure 5 shows the input and fit directional spectra for the base case in no current, computed using the developed framework and the commonly used MEP approach. The spectra in Fig. 5 show: the input spectrum; the computed directional spectrum using the present framework and the theoretical cross-spectra; the computed directional spectrum using the present framework and the synthesized surface elevation time-series; and the computed directional spectrum using the MEP approach and the same synthesized surface elevation time-series. From the spectra, it can be observed that the framework developed here closely matches the MEP method and differences from the input directional spectra arise due to the method employed to synthesize the surface elevation time-series as demonstrated by the difference between the theoretical cross-spectra and time series cross-spectra and the close agreement between the theoretical cross-spectra and the input directional spectrum.

To determine the accuracy of the present framework, the normalized error in the estimated directional spectra ($E(f,\theta)_e$) relative to the input directional spectra ($E(f,\theta)_i$) was computed:

$$\mu = \frac{\sum_{f\in\mathbb{F}}\sum_{\theta=0}^{2\pi}|E(f,\theta)_e - E(f,\theta)_i|}{\sum_{f\in\mathbb{F}}\sum_{\theta=0}^{2\pi}E(f,\theta)_i} \tag{29}$$

Figure 6 shows the error in the directional spectra normalized by the total energy ($\mu$) and again highlights that the present framework is capable of accurately estimating the parameters with errors below 10% for a range of directional spreads and wave periods. Compared to the Newton MEP method, the present framework can produce comparable results with improvements in particular observed for high spread values.

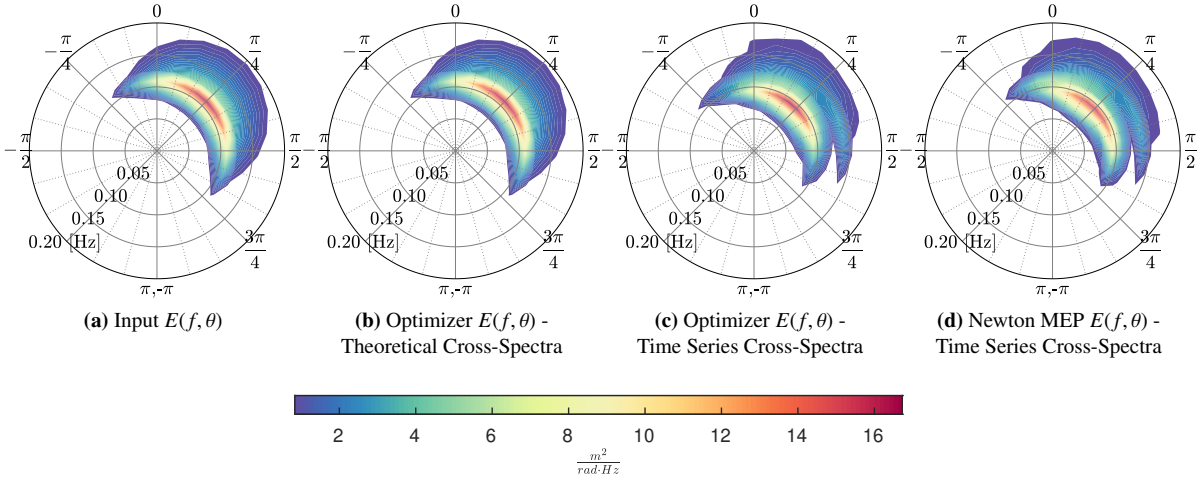


**(a)** Input $E(f,\theta)$

**(b)** Optimizer $E(f,\theta)$ - Theoretical Cross-Spectra

**(c)** Optimizer $E(f,\theta)$ - Time Series Cross-Spectra

**(d)** Newton MEP $E(f,\theta)$ - Time Series Cross-Spectra

**Figure 5:** Example Directional Spectra composed of a JONSWAP spectrum with $H_s = 4\,\text{m}$ and $T_p = 9.5\,\text{s}$ and spreading function based on a cos-2s function with $s = 5$, $\theta_0 = \frac{\pi}{4}\ rad$.

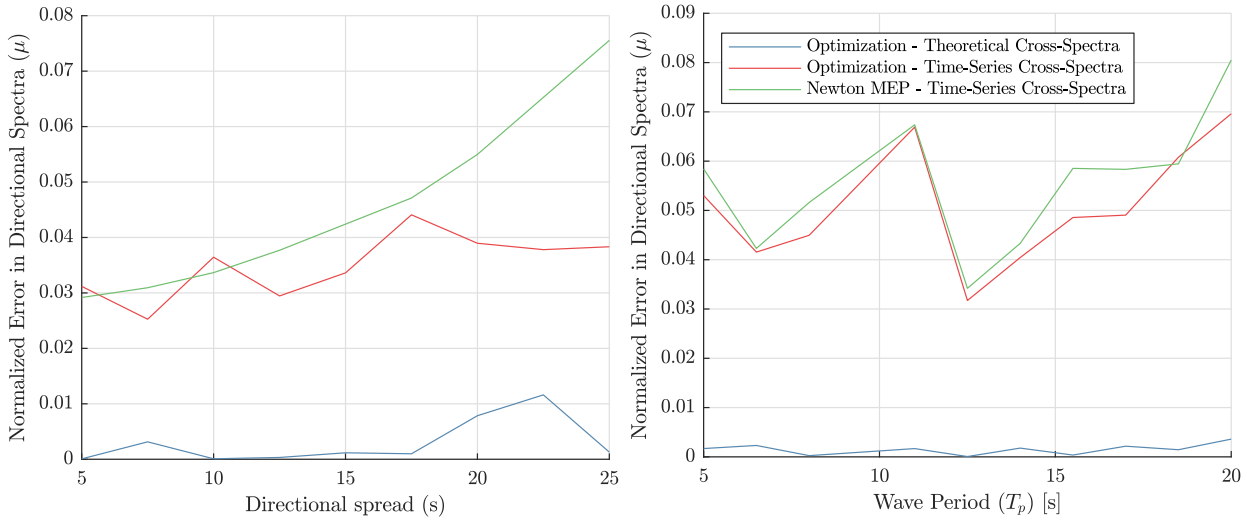


**(a)**

**(b)**

**Figure 6:** Normalized error in the fit directional spectra relative to the total energy. The time-series cross-spectra are used for the optimization approach and the Newton MEP case. Both have errors of less than 10% for a range of directional spread and wave periods. Applying the optimization solver to the theoretical cross-spectra yields even lower errors on the order of 0.1%

Figure 7 shows the fitted cos-2s parameters compared to the input parameters showing close agreement between the known conditions and those estimated by the optimization. For each case, the theoretical cross-spectra lead to a more accurate estimate as would be expected as these contain no spectral leakage or sampling sensitivities. It is noted that the spread variables show higher variation than the mean direction which is very accurately estimated.

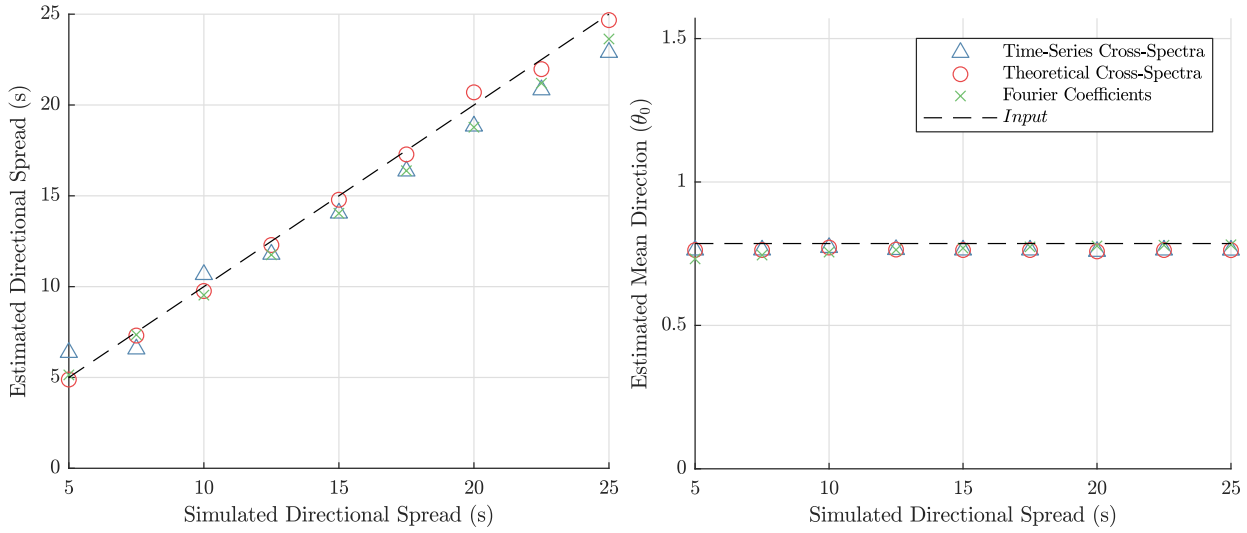


**Figure 7:** Fitted directional spreading function parameters (energy weighted average over the frequencies) compared to those simulated. The $s$ values (shown in (a)) represent the spread and the values in (b) represent the mean direction, $\theta_0$ for a unidirectional cos-2s spreading function. All cases consider no current, and a JONSWAP spectrum with $H_s = 4\,\text{m}$ and $T_p = 9.5\,\text{s}$ and spreading function based on a cos-2s, $\theta_0 = \frac{\pi}{4}$ *rad*. For each case, the cos-2s parameters are fitted using the present method and either the theoretical cross-spectra or the simulated time-series cross-spectra representing the sea state. From the simulated time-series, the parameters are commonly computed using a Fourier Coefficient method which is also shown for comparison.

### *3.3. Bimodal Directional Spread in the Presence of Current*

As the framework was developed allowing sufficient flexibility to consider bimodal directionally spread seas and the presence of current, a case was run using the same base parameters shown in Table 2, but with the inclusion of a second mode defined by $s_2$, $\phi_0$ and $\lambda$:

**Table 3:** Bimodal Case Parameters

| $s_1$ | $\theta_0$ | $s_2$ | $\phi_0$ | $\lambda$ | U | $\beta$ |
|---|---|---|---|---|---|---|
| 5 | 0 rad | 10 | $\frac{\pi}{2}$rad | 0.5 | $0.4\,\text{m}\,\text{s}^{-1}$ | 0 rad |

Deploying the parameter estimation framework to the synthesized cross-spectra for this case yields the directional spectra shown in Fig. 8. From this figure, it can be seen that the optimization framework correctly identifies both modes of the spectra similar to the Newton MEP approach.

Compared to the unimodal case shown in Fig. 5, the directional spectra is not as well resolved. However, given the increased complexity of the conditions (multi-modal waves and current) this is not unexpected. The optimization output at each frequency is shown in Fig. 9 with the energy spectra superimposed. From this figure it can be seen that for the high energy portions of the spectrum, the method quite accurately identifies the parameters (i.e. values close to the target values: $s_1 = 5$, $\theta_0 = 0\,\text{rad}$, $s_2 = 10$, $\phi_0 = \frac{\pi}{2}\text{rad}$). At both low and high frequencies, where there is less energy in the system, the parameters are not as well isolated. In general, as the optimizer is considering very small changes to the cross-spectra, the impact of the current at frequencies at which there is little energy therefore has almost negligible impact on the objective function. It can therefore be difficult for the optimizer to accurately isolate as demonstrated by the erroneous peak in current speed at 0.156 Hz. For the present study, each frequency used the same convergence criteria, however, the framework allows flexibility (as shown in Fig. 4) enabling this convergence to be defined as a function of the relative energy at a given frequency component. Defining the convergence threshold in this way would allow high-frequency, low-energy, components to utilise a smaller convergence threshold. Though this would require greater computational time, it would better resolve the high frequency components of the spectra reducing the high frequency errors.

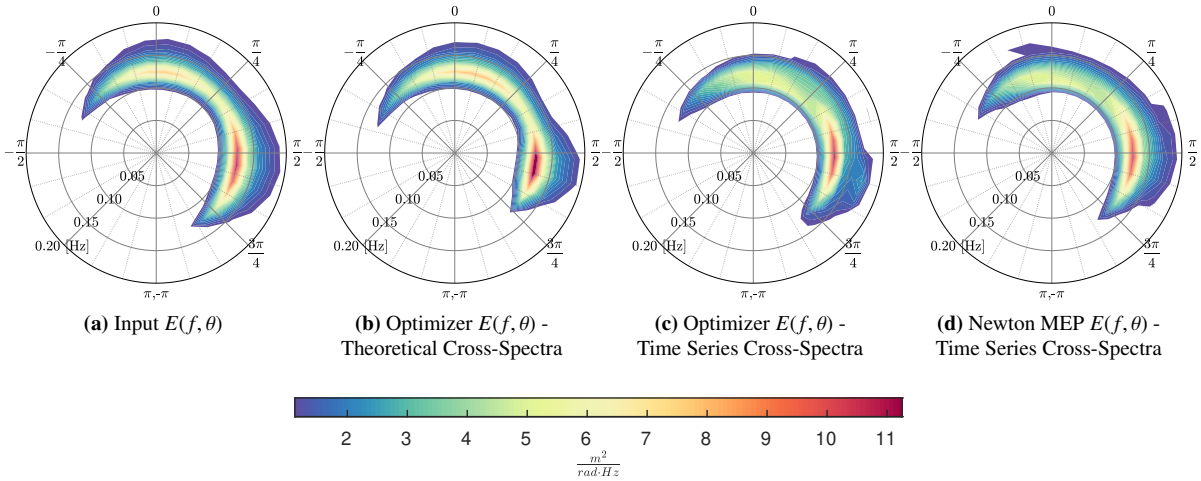


**(a)** Input $E(f, \theta)$

**(b)** Optimizer $E(f, \theta)$ - Theoretical Cross-Spectra

**(c)** Optimizer $E(f, \theta)$ - Time Series Cross-Spectra

**(d)** Newton MEP $E(f, \theta)$ - Time Series Cross-Spectra

**Figure 8:** Example Directional Spectra with $s_1 = 5$, $\theta_0 = 0\,\text{rad}$, $s_2 = 10$, $\phi_0 = \frac{\pi}{2}\text{rad}$ with $\lambda = 0.5$ (i.e. equal weight between the two modes), and a current speed of $0.40\,\text{m s}^{-1}$ from a direction, $\beta$, of 0 rad

### *3.4. Unimodal Directional Spectra in the Presence of Current*

Table 2 describes the full range of the 125 simulations completed for this study. Of these, 20 simulations were done with no current, while the remaining 105 simulations were executed for different current speeds and mean wave directions using the base case with unimodal directional spread. The current direction was not changed, as the sensitive parameter is the relative angle between the waves and currents. Directional spectra estimates for one the simulations are shown in Fig. 10 for a case where the current is $1.00\,\text{m s}^{-1}$ and the waves are at $\frac{\pi}{2}$ rad to the current which has a direction of 0 rad. The corresponding optimizer outputs for each frequency are shown

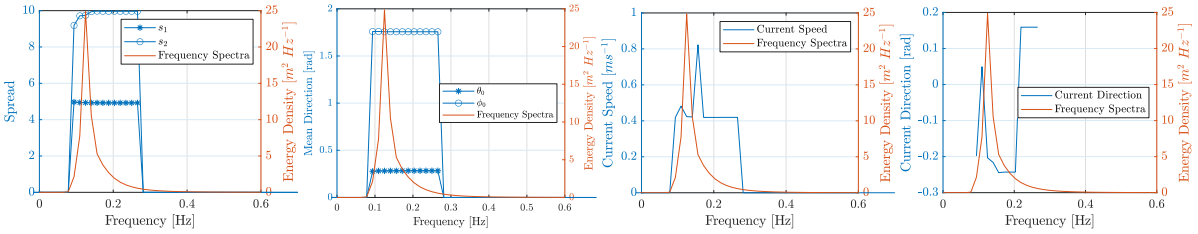


**(a)** cos-2s Spread **(b)** cos-2s Mean Direction **(c)** Current Speed **(d)** Current Direction

**Figure 9:** Spread and current spectra from optimization output using time-series cross-spectra for bimodal case of $s_1 = 5$, $\theta_0 = 0\,\text{rad}$, $s_2 = 10$, $\phi_0 = \frac{\pi}{2}\,\text{rad}$ with $\lambda = 0.5$ (i.e. equal weight between the two modes), and a current speed of $0.40\,\text{m}\,\text{s}^{-1}$ from a direction, $\beta$, of $0\,\text{rad}$. In each plot, the sea state energy density is shown in red.

in Fig. 11. As the solver operates frequency by frequency, it identifies directional spreading parameters and current parameters associated with each frequency. This figure shows the converged results corresponding to the solution shown in Fig. 10c for a unimodal case ($s_1 = 5$, $\theta_0 = \frac{\pi}{2}$ *rad*, $U = 1.00\,\text{m}\,\text{s}^{-1}$, and $\beta = 0\,\text{rad}$). From this figure it can be observed that across all frequencies where there is significant wave energy, the optimizer accurately identifies the correct parameters despite the fact that the wave-current interaction is minimal at this relative angle.

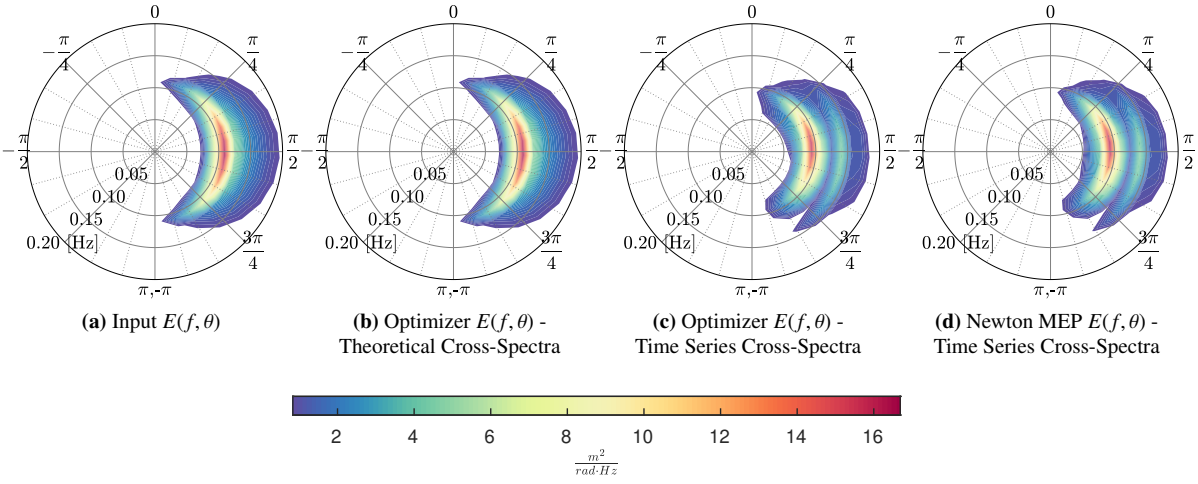


**(a)** Input $E(f,\theta)$ **(b)** Optimizer $E(f,\theta)$ - Theoretical Cross-Spectra **(c)** Optimizer $E(f,\theta)$ - Time Series Cross-Spectra **(d)** Newton MEP $E(f,\theta)$ - Time Series Cross-Spectra

**Figure 10:** Example Directional Spectra with $s_1 = 5$, $\theta_0 = \frac{\pi}{2}$ *rad*, $U = 1.00\,\text{m}\,\text{s}^{-1}$, and $\beta = 0\,\text{rad}$

Considering the full set of simulations, the estimated current speeds and directions are shown in Fig. 12 with the root mean square error (RMSE) by relative angle between the waves and current shown in Table 4. These values represent the energy-weighted mean obtained over the directional spectrum. From this plot and the corresponding table it can be seen that the largest errors in the current speed are for a relative angle of $\frac{\pi}{2}$ rad at which there is theoretically minimal interaction between the waves and current. This is not unexpected, as the entire framework is premised on using the current's impact on wavenumbers to resolve both the current and the DSF. In scenarios of weak wave-current interaction, this impact of the current on the wavenumbers is small and

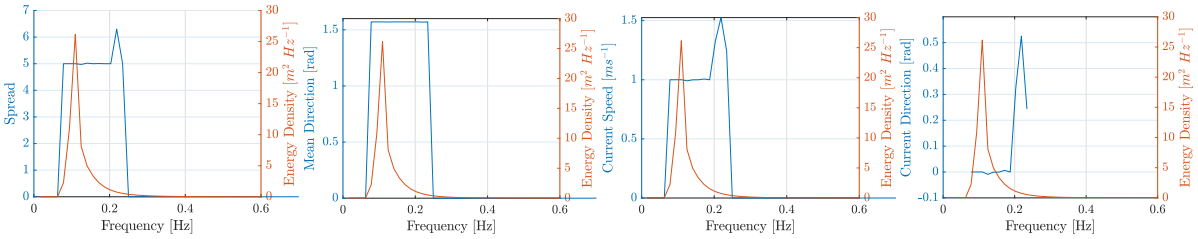


**(a)** cos-2s Spread **(b)** cos-2s Mean Direction **(c)** Current Speed **(d)** Current Direction

**Figure 11:** Spread and current spectra from optimization output using time-series cross-spectra for unimodal case of $s = 5$, $\theta_0 = \frac{\pi}{2}$rad, $U = 1.00\,\mathrm{m\,s^{-1}}$, and $\beta = 0$ rad. In each plot, the sea state energy density is shown in red.

therefore the optimization error function is relatively insensitive to the current velocity. In general, however, it is clear that the framework is able to predict the current speed and direction well in all cases.

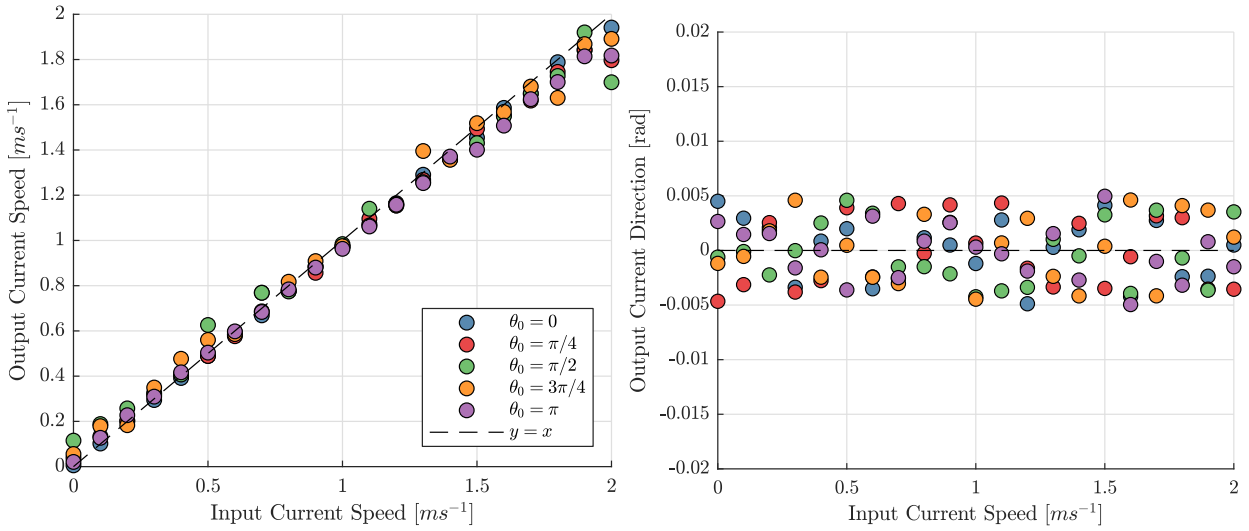


**(a)** Speed **(b)** Direction

**Figure 12:** Estimation of Current from Wave Buoy Measurements

The corresponding root mean square errors for the estimated wave and current parameters considering all the cases with and without current are reported in Table 5. Noticeably, when considering all the cases with and without current, a higher RMSE in current velocity is observed to that reported in Table 4. This is due to the optimization framework having higher errors at low current speeds due to the manner in which the objective function is impacted by the current estimate. In general, all parameters are estimated acceptably well, with the mean wave and current directions particularly well predicted when a current is present.

As discussed in Section 2.1 and highlighted in Fig. 1, the presence of an ignored current can result in significant errors in both estimates of the wave power and wave steepness. Figure 13 shows the estimated relative wave power and steepness (ratio of estimated values to the theoretical

**Table 4:** RMSE in Current Estimation

| | $\theta_0$ [rad] | | | | |
|---|---|---|---|---|---|
| | 0 | $\frac{\pi}{4}$ | $\frac{\pi}{2}$ | $\frac{3\pi}{4}$ | $\pi$ |
| $U$ [m s$^{-1}$] | 0.0300 | 0.0588 | 0.0871 | 0.0619 | 0.0637 |
| $\beta$ [rad] | 0.0028 | 0.0032 | 0.0028 | 0.0030 | 0.0025 |

**Table 5:** RMSE of Estimated Parameters Across All Simulations

| | RMSE | |
|---|---|---|
| **Parameter** | **Theoretical** | **Time Series** |
| $s_1$ | 0.3201 | 1.5123 |
| $\theta_0$ [rad] | 0.0941 | 0.1882 |
| $U$ [m s$^{-1}$] | 0.0002 | 0.1179 |
| $\beta$ [rad] | 0.0029 | 0.0091 |

values assuming linear wave-current interaction theory) using the present developed framework and integrated over frequency components for each case (solid lines) compared to what would have been estimated using the traditional Newton MEP approach (dotted lines). As can be observed, by accurately characterising both the waves and currents, the power and steepness are now more accurately computed (i.e. close to values of 1.0). The greatest errors are now reduced from on the order of 30% to a maximum of 3%.

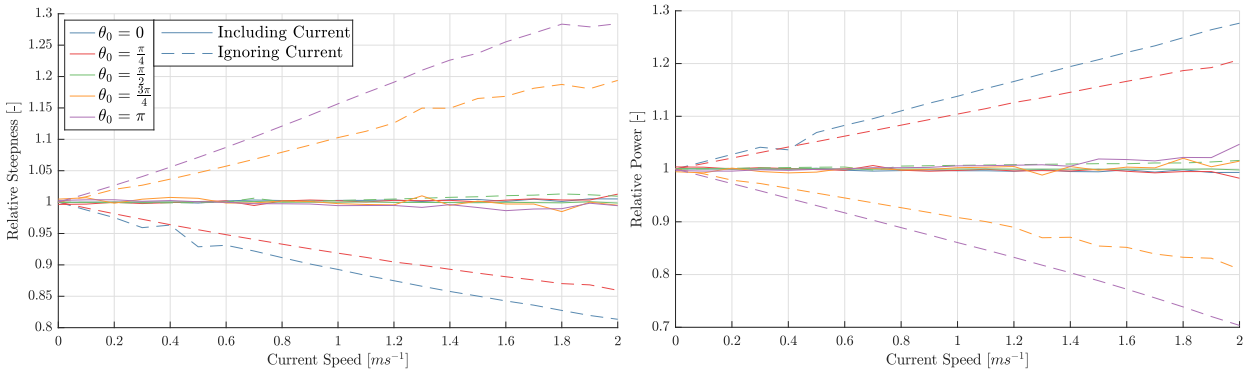


**(a)** Wave Steepness **(b)** Wave Power

**Figure 13:** Relative wave steepness and power; solid lines show the relative steepness and power estimated using the present framework for a range of current speeds and directions and the dotted lines show the relative steepness and power estimated using a Newton MEP approach.

## 4. Discussion & Future Work

### *4.1. Method performance*

Overall, the devised framework for processing wave buoy data in the presence of current has been found to accurately estimate the underlying directional spectrum and current velocity across a range of simulated data. In the case of no current, the method has similar errors to the established Newton MEP approach with errors less than 5% in spread and less than 10% in mean direction. In the absence of current and at low current speeds below approximately $0.4\,\mathrm{m\,s^{-1}}$, the method has a tendency to over-predict the current speed due to the relatively small impact that incorrect current estimates have on the optimizer's objective function. In the presence of higher currents above approximately $0.4\,\mathrm{m\,s^{-1}}$, the framework accurately estimates both wave and current parameters over a wide range of directional combined wave-current conditions, with good performance additionally demonstrated for multi-modal sea states. This enables the sea state power and steepness to be accurately inferred which are of critical importance for the design and operation of offshore structures and devices.

The current implementation of the framework, although effective, is relatively slow (requiring between 3.9 and 12.9 times longer than the Newton MEP and 5.9 times longer on average). This range in computational time compared to the Newton MEP is driven by a number of factors. These include principally if the DSF is unimodal or bimodal; though the same implementation is used for both, as the initial guess is unimodal ($\lambda = 0$) these solutions converge the quickest. A weak relationship to the current velocity was also observed with cases where the current opposed the waves taking slightly longer to converge. Higher current velocities were also observed to consistently require greater computational time. This is not unexpected as the interacting effects are increased in these situations thereby requiring greater searching to converge. Section 2.4 explains that the initial guess at each frequency component is initialized to the solution at the previous frequency component. This was done as it was found to significantly reduce computational time (with no impact to the converged solution) by effectively warm-starting the solver to a sensible guess close to the solution.

Future work will look to speed this up using two approaches. Firstly, as the framework is solving for parameters frequency by frequency under the assumption of linearity, then the code can be readily parallelised. Secondly, it is thought that using the Newton MEP approach to provide the initial estimates could help find a solution much quicker. It is evident that the directional spectra produced by the MEP are actually very close to the target (as expected from Fig. 2) and hence this would serve as a good initial guess for the DSF allowing the optimization approach to focus on solving for the current velocity. Furthermore, the present implementation solves the frequencies in ascending order, starting instead at the peak frequency where the highest energy is present could improve the optimization speed for the remaining frequencies as this solution would be used as a starting point.

### *4.2. Effect of current-modified buoy dynamics*

In order to test the method performance, a simplified method was used to simulate the buoy motions in which it was assumed that the buoy perfectly tracked the water surface. Even without a current it is common practice to use frequency-dependent buoy-specific transfer functions in order

to convert from the buoy motions to that of the true water surface [15]. If these are relatively linear, they can be accounted for by simple inclusion in the formulation of the estimated cross-spectra (e.g. Eq. (27)). The buoy response in current, however, becomes more complex as discussed in Section 1. Of particular importance is that the mooring will become taut in significant currents, which means the buoy response can no longer be considered as uncoupled to the mooring. This may alter the dynamics significantly, and for some mooring configurations, will also alter the buoy draught. This added complexity associated with the mooring is in addition to the current-induced drag on the buoy itself and the potential for vortex-induced motions [45, 46] which, if significant, will alter the spatial sampling of the wave field.

It is expected that the various factors will result in a complex set of non-linear transfer functions which are highly sensitive to current velocity and the specifics of the mooring configuration. Further work, including experiments at the FloWave basin in Edinburgh, will aim to assess the relative influence of the modified buoy dynamics on the buoy motions and resulting processed outputs. This will allow an assessment to be made as to whether this is significant, and if so, whether they can properly account for in the newly developed framework. Importantly, this will also help quantify the true uncertainty in ocean data obtained from wave buoys in the presence of a current.

### *4.3. Dealing with complex current fields*

Throughout this work we have assumed that the current is both uniform and steady. Real currents, however, are often characterised as turbulent due to short-term fluctuations and frequently have a notable vertical shear profile. Additionally, the mean current itself varies over relatively short time frames ($O$(mins)) with the state of the tide. If the mean current is relatively constant, then the effect of turbulence on the analysis can be negated as spectral values can be taken over reasonably long time frames (e.g. 30 mins). However, if the mean current is changing rapidly, then shorter time-frames will need to be used for spectral analysis to ensure the wave statistics are stationary. Further work is hence required to assess this trade-off and identify appropriate time-frames for spectral analysis in the presence of varying and turbulent current fields.

Vertical shear also adds complexity, in part due to more complex wave-current interaction. Of specific relevance for this work is that there is a modified dispersion relation, whereby wave components of different frequencies effectively 'observe' a different current velocity (e.g. Yao and Wu [47]). Higher frequency components, with higher wavenumbers, will only effectively interact with the current velocities in the upper water column. In the current framework, this means that a simple weighted mean current may not be an adequate description of the current field. The authors suggest that it may be possible to estimate the current profile by the frequency-dependent differences in the 'effective' current velocities calculated. This possibility will be explored in future work.

### *4.4. Dealing with arbitrary shaped directional spectra*

The presented approach for calculating the DSF is based on calculating parameters for a bimodal cos-2s formulation. This allows for two separate symmetrical directional modes, or one asymmetric mode; where the two modes are overlapping to create asymmetric shapes. This approach should be valid for the majority of sea states, however, it is acknowledged that certain

scenarios may occur where two asymmetric modes may co-exist. Future work will initially explore the occurrence of such conditions to assess the potential impact of this, before assessing whether other DSF formulations may be proposed which can account for a wider range of shapes. This will inevitably include additional parameters, which may affect performance, and hence it will only be implemented if it is required.

### *4.5. Applications*

As discussed above there are a number of areas of future work before the method is refined and full confidence is gained in the application to real ocean data. It is expected that the main challenges arise in quantifying and dealing with changes to the buoy dynamics in current (Section 4.2). If these are accounted for, or deemed negligible for the outputs of the framework, then the methodology can be applied to real ocean datasets opening up a wide range of potential applications.

As part of our future work in addition to the scale testing at Flowave, a study using a dataset of a co-located wave buoy an acoustic Doppler current profiler (ADCP) off the coast of the UK will be used to test and verify the method's validity to ocean data. The ADCP will provide an accurate measure of the current velocity enabling direct comparison against the present framework and a full verification of the framework using real ocean data.

The potential to properly account for current in ocean datasets has significant and wide-ranging implications. A re-assessment of global wave buoy datasets would enable improved estimates of the sea state steepness and power to be obtained, which in turn, will reduce uncertainty in the design and operation of offshore systems. Of particular relevance may be wave energy converters (owed to their large dynamic response), where knowledge of the sea state steepness, directionality and power is of critical importance for both design and performance assessment.

If applied widely, the estimation of current velocity from wave buoys will also provide a separate current velocity dataset for a wide range of global locations where data doesn't currently exist. This may be used to calibrate/validate numerical models as well as being used directly for offshore design.

Additionally, once the directional spectra and the current velocity are both known, then it is also possible to estimate what the directional spectrum would be without the current; accounting for conservation of wave action and refraction effects [48]. This then provides proper benchmark datasets for the validation of spectral wave models, where previously they will be calibrated and validated against datasets which are affected by an unknown current.

## 5. Conclusions

Wave buoy data is routinely used for the design of offshore structures and devices. However, wave buoys do not measure current and as such the ocean conditions have considerable uncertainty: wave steepness, power and wavelengths are incorrectly calculated, and the current remains unknown. The theoretical errors are presented in this paper and demonstrate that for higher frequency waves the errors in sea state power and steepness may be greater than $\pm 40\%$ for $\pm 2$ ms$^{-1}$.

To resolve this problem we present a framework able to calculate the current and current-modified wave parameters from wave buoy motions alone. The methodology uses a theoretical

formulation of the cross-spectra which includes the directional spectrum and the current-modified wave parameters, which is used in combination with measured cross-spectra between heave, surge, and sway motions. A Mesh Adaptive Direct Search (MADS) algorithm is used to minimize the error between the estimated and measured cross-spectra to solve for all parameters. On simulated wave buoy motion data the method is shown to be effective over a range of combined wave-current sea states; providing reliable estimates of current velocity, current direction, directional spread & mean direction (of up to 2 modes) for each frequency component. This results in errors in sea state power and steepness of less than ±3% for all 125 test cases.

Following validation for wave buoy datasets, the framework has the capability to improve the quality of all historic and active wave buoy deployments where there is notable current. Improved values of wave parameters will be obtained in addition to providing new datasets of current velocity in a wide range of locations. Both the wave and current parameters are of critical importance for offshore design, and hence improved loading estimates will be obtained which can be used to reduce safety factors (and cost) and/or provide more appropriate design solutions for the environmental conditions.

## Acknowledgements

This work is funded in part by the EPSRC Supergen Offshore Renewable Energy Hub [grant no: EP/S000747/1] Flexible Fund support for *Accounting for Current in Wave Buoy Measurements*. S. Draycott acknowledges a Dame Kathleen Ollerenshaw Fellowship.

## References

[1] J. Wolf, D. Prandle, Some observations of wave-current interaction, Coastal Engineering 37 (1999) 471–485. doi:10.1016/S0378-3839(99)00039-3.

[2] S. Draycott, A. C. Pillai, D. M. Ingram, L. Johanning, Resolving combined wave-current fields from measurements using interior point optimization, Coastal Engineering 149 (2019) 4–14. URL: https://doi.org/10.1016/j.coastaleng.2019.03.008. doi:10.1016/j.coastaleng.2019.03.008.

[3] M. Tucker, E. Pitt, Waves in Ocean Engineering, Voume 5 (Elsevier Ocean Engineering Series), Elsevier Science, 2001.

[4] NOAA NDBC, National Data Buoy Center, 2011.

[5] NOAA, National Oceanic and Atmospheric Adminstration National Centers for Environmental Information, 2020. URL: https://www.nodc.noaa.gov/BUOY/.

[6] Cefas, Cefas - WaveNet, 2019. URL: https://www.cefas.co.uk/cefas-data-hub/wavenet/.

[7] F. I. Gonzales, A Case Study of Wave-Current-Bathymetry Interactions at Columbia River Entrance, Journal of Physical Oceanography 14 (1984) 1065–1078.

[8] H. L. Tolman, Effects of Tides and Storm Surges on North Sea Wind Waves, Journal of Physical Oceanography 21 (1990) 766–781.

[9] D. W. Wang, A. K. Liu, Y. P. Chih, E. A. Meindl, Wave-current interaction near the Gulf Stream during the Surface Wave Dynamics Experiment, Journal of Geophysical Research 99 (1994) 5065–5079. doi:10.1029/93JC02714.

[10] D. Masson, A Case Study of Wave-Current Interaction in a Strong Tidal Current, Journal of Physical Oceanography 26 (1996).

[11] C. Macisaac, S. Naeth, TRIAXYS Next Wave II Directional Wave Sensor The Evolution of Wave Measurements, 2013 OCEANS - San Diego (2013) 1–8. doi:10.23919/OCEANS.2013.6741003.

[12] Y. Pérignon, J. Thomson, A. Benetazzo, P. Sutherland, P. Ferrant, P. Veras Guimarães, M. Accensi, F. Ardhuin, M. Hamon, A surface kinematics buoy (SKIB) for wave–current interaction studies, Ocean Science 14 (2018) 1449–1460. doi:10.5194/os-14-1449-2018.

[13] I. G. Jonsson, C. Skougaard, J. D. Wang, Interaction Between Waves and Currents, Coastal Engineering 1970 (1970) 489–507. doi:10.2307/j.ctvfrxqp9.34.

[14] M. Benoit, P. Frigaard, H. A. Schaäffer, Analysing Multidirectional Wave Spectra: a Tentative Classification of Available Methods, Proceedings IAHR Seminar on Multidirectional Waves and their Interaction whith Structures (1997) 131–154.

[15] M. D. Earle, Nondirectional and Directional Wave Data Analysis Procedures. NDBC Technical Document 96-01, Technical Report January, Stennis Space Center, 1996.

[16] K. E. Steele, Ocean current kinematic effects on pitch-roll buoy observations of mean wave direction and nondirectional spectra, Journal of Atmospheric and Oceanic Technology 14 (1997) 278–291. doi:10.1175/1520-0426(1997)014¡0278:OCKEOP¿2.0.CO;2.

[17] E. K. Burke, G. Kendall, Search Methodologies, second ed., Springer US, Boston, MA, 2013. doi:10.1007/0-387-28356-0.

[18] Y. Bard, Nonlinear Parameter Estimation, Academic Press, 1974.

[19] W. R. Esposito, C. A. Floudas, Global optimization in parameter estimation of nonlinear algebraic models via the error-in-variables approach, Industrial and Engineering Chemistry Research 37 (1998) 1841–1858. doi:10.1021/ie970852g.

[20] W. R. Esposito, C. A. Floudas, Global optimization for the parameter estimation of differential- algebraic systems, Industrial and Engineering Chemistry Research 39 (2000) 1291–1310. doi:10.1021/ie990486w.

[21] S. D. Weller, S. J. Banfield, J. Canedo, Parameter estimation for synthetic rope models, Proceedings of the International Conference on Offshore Mechanics and Arctic Engineering - OMAE 1 (2018). doi:10.1115/OMAE2018-78606.

[22] D. Peregrine, Interaction of Water Waves and Currents, in: C.-S. Yih (Ed.), Advances in Applied Mathematics, volume 16 of *Advances in Applied Mechanics*, Elsevier, 1976, pp. 9–117. URL: http://www.sciencedirect.com/science/article/pii/S0065215608700875. doi:https://doi.org/10.1016/S0065-2156(08)70087-5.

[23] M. Isobe, K. Kondo, K. Horikawa, Extension of MLM for estimating directional wave spectrum, Proceedings of the Symposium on Description and Modeling of Directional Seas (1984).

[24] N. Hashimoto, K. Kobune, Directional spectrum estimation from a Bayesian approach, Proceedings of the 21st International Conference on Coastal Engineering June 20-25, 1988, Costa del Sol-Malaga, Spain (1988) 62–76.

[25] H. Mitsuyasu, F. Tasai, T. Suhara, S. Mizuno, M. Ohkusu, T. Honda, K. Rikiishi, Observations of the directional spectrum of ocean waves using a coverleaf buoy, Journal of Physical Oceanography 5 (1975) 750–760. doi:10.1175/1520-0485(1975)005¡0750:OOTDSO¿2.0.CO;2.

[26] M. Longuet-Higgins, D. Cartwright, N. Smith, Observations of the Directional Spectrum of Sea Waves Using the Motions of a Floating Buoy, Ocean Wave Spectra (1961).

[27] K. Hasselmann, T. P. Barnett, E. Bouws, H. Carlson, D. E. Cartwright, K. Eake, J. A. Euring, A. Gicnapp, D. E. Hasselmann, P. Kruseman, A. Meerburg, P. Mullen, D. J. Olbers, K. Richren, W. Sell, H. Walden, Measurements of wind-wave growth and swell decay during the joint North Sea wave project (JONSWAP)., Technical Report January, Deutsches Hydrographisches Institut - Hamburg, 1973.

[28] M. Benoit, Practical Comparative Performance Survey of Methods Used for Estimating Directional Wave Spectra From Heave-Pitch-Roll Data, Coastal Engineering (1992) 62–75.

[29] M. Miles, E. Funke, A Comparison of Methods for Synthesis of Directional Seas, Journal of Offshore Mechanics and Arctic Engineering 111 (1989) 247–255.

[30] S. Draycott, T. Davey, D. M. Ingram, A. Day, L. Johanning, The SPAIR method: Isolating incident and reflected directional wave spectra in multidirectional wave basins, Coastal Engineering 114 (2016) 265–283. doi:10.1016/j.coastaleng.2016.04.012.

[31] S. Draycott, D. R. Noble, T. Davey, T. Bruce, D. M. Ingram, L. Johanning, H. C. Smith, A. Day, P. Kaklis, Re-creation of site-specific multi-directional waves with non-collinear current, Ocean Engineering 152 (2018) 391–403. doi:10.1016/j.oceaneng.2017.10.047.

[32] B. Craenen, A. Eiben, E. Marchiori, How to Handle Constraints with Evolutionary Algorithms, Practical Handbook Of Genetic Algorithms: Applications, Second Edition (2001).
[33] K. Deb, An Efficient Constraint Handling Method for Genetic Algorithms, Computer Methods in Applied Mechanics and Engineering 186 (1998) 311—-338. doi:10.1016/S0045-7825(99)00389-8.
[34] C. A. Coello Coello, E. M. Montes, Constraint-handling in genetic algorithms through the use of dominance-based tournament selection, Advanced Engineering Informatics 16 (2002) 193–203. doi:10.1016/S1474-0346(02)00011-3.
[35] R. Hooke, T. A. Jeeves, "Direct Search" Solution of Numerical and Statistical Problems, Journal of the ACM 8 (1961) 212–229.
[36] J. Larson, M. Menickelly, S. M. Wild, J. Larson, M. Menickelly, S. M. Wild, Derivative-free optimization methods, Acta Numerica 28 (2019) 287–404.
[37] S. S. Rao, Engineering Optimization: Theory and Practice, fourth ed., John Wiley & Sons, Hoboken, New Jersey, 2009. doi:10.1002/9780470549124.
[38] A. Wächter, L. Biegler, On the implementation of a interior point filter line search algorithm for large-scale nonlinear programming, Mathematical Programming 106 (2006) 25–57.
[39] M. H. Wright, The interior-point revolution in optimization: History, recent developments, and lasting consequences, Bulletin of the American Mathematical Society 42 (2005) 39–56. doi:10.1090/S0273-0979-04-01040-7.
[40] C. Audet, J. J. Dennis, Mesh adaptive direct search algorithms for constrained optimization, SIAM Journal on Optimization 17 (2006) 188–217.
[41] S. Le Digabel, Algorithm 909: NOMAD: Nonlinear optimization with the MADS algorithm, ACM Transactions on Mathematical Software 37 (2011). doi:10.1145/1916461.1916468.
[42] M. A. Abramson, C. Audet, J. W. Chrissis, J. G. Walston, Mesh adaptive direct search algorithms for mixed variable optimization, Optimization Letters 3 (2009) 35–47. doi:10.1007/s11590-008-0089-2.
[43] C. Audet, G. Savard, W. Zghal, A mesh adaptive direct search algorithm for multiobjective optimization, European Journal of Operational Research 204 (2010) 545–556. doi:10.1016/j.ejor.2009.11.010.
[44] N. Hashimoto, Analysis of the directional wave spectrum from field data, Advances in coastal and ocean engineering 3 (1997) 103–144.
[45] R. N. Govardhan, C. H. Williamson, Vortex-induced vibrations of a sphere, Journal of Fluid Mechanics 531 (2005) 11–47. doi:10.1017/S0022112005003757.
[46] A. Sareen, J. Zhao, J. Sheridan, K. Hourigan, M. C. Thompson, Vortex-induced vibrations of a sphere close to a free surface, Journal of Fluid Mechanics 846 (2018) 1023–1058. doi:10.1017/jfm.2018.290.
[47] A. Yao, C. H. Wu, Incipient breaking of unsteady waves on sheared currents, Physics of Fluids 17 (2005) 1–10. doi:10.1063/1.2000276.
[48] I. G. Jonsson, O. Skovgaard, Wave Refraction Across a Shearing Current., Proceedings of the Coastal Engineering Conference 1 (1979) 722–741.